# Controlling the diversity of ion-induced fragmentation pathways by N -methylation of amino acids

Darío Barreiro-Lage, Chiara Nicolafrancesco, Jaroslav Kočišek, Alberto Luna, Janina Kopyra, Manuel Alcamí, Bernd Huber, Fernando Martín, Patrick Rousseau, Sergio Díaz-Tendero, et al.

# Controlling the diversity of ion-induced fragmentation pathways by $N-$methylation of amino acids†

Darío Barreiro-Lage,[a] Chiara Nicolafrancesco,[b,c] Jaroslav Kočišek,[d] Alberto Luna,[e] Janina Kopyra,[f] Manuel Alcamí,[a,g,h] Bernd A. Huber,[b] Fernando Martín,[a,g,i] Alicja Domaracka,[b] Patrick Rousseau,*[,b] Sergio Díaz-Tendero,*[,a,h,i]

We present a combined experimental and theoretical study of the fragmentation of singly and doubly $N-$methylated glycine (sarcosine and $N,N-$dimethyl glycine, respectively) induced by low-energy (keV) $O^{6+}$ ions. Multicoincidence mass spectrometry techniques and quantum chemistry simulations (*ab initio* molecular dynamics and density functional theory) allow us to characterise different fragmentation pathways as well as the associated mechanisms. We focus on the fragmentation of doubly ionised species, for which coincidence measurements provide unambiguous information on the origin of the various charged fragments. We have found that single $N-$methylation leads to a larger variety of fragmentation channels than in no methylation of glycine, while double $N-$methylation effectively closes many of these fragmentation channels, including some of those appearing in pristine glycine. Importantly, the closure of fragmentation channels in the latter case does not imply a protective effect by the methyl group.

## 1 Introduction

Miller-Urey experiment on the synthesis of organic compounds under primordial-Earth conditions is considered one of the foremost experiments of the twentieth century. He sent an electrical charge through a flask containing a chemical solution composed of methane, ammonia, hydrogen and water. Starting from this mixture of primary gases, and using the electrical discharges as an energy source, he was able to synthetise several amino acids and amine-derivatives back in 1953[1]. The premise that those amino acids could be seen as the precursors of larger organic molecules was reinforced in 1969, when a type II carbonaceous chondrite fell in Murchinson. After chemical analysis, Kvenvolden et al. reported that a large amount of amino acids was present on it[2], and that most of them were similar to those synthesised in Miller's experiment. Today, amino acids have been also detected in interplanetary dust particles[3]; as they rain down on a planet surface, they import the possible building blocks for life formation. In such media, they are exposed to ionising radiation; it is therefore interesting to study their behaviour when they are ionised and excited. Even doubly-ionised species have been reported to be involved in the formation of new bio-molecules in the interstellar media or even in planet atmospheres[4].

From a biological point of view, a deep understanding of the effect of ionising radiation in amino acids can be useful to identify the primary mechanisms leading to radiation damage in peptides, proteins, and ultimately to biological tissues[5,6]. In this respect, experiments on biologically relevant molecules interacting with ionising radiation in the gas-phase can provide quite useful insight[7–18]. Ionised amino acids have been shown to follow specific fragmentation pathways arising from a large variety of mechanisms. Being very relevant in gas phase ionic chemistry, the dynamics and mechanisms leading to their fragmentation after ionisation have been the subject of intense research in the last years, where the formation of radical species have been reported[4,16,19–23].

[a] *Departamento de Química, Módulo 13, Universidad Autónoma de Madrid, 28049 Madrid, Spain*
[b] *Normandie Univ, ENSICAEN, UNICAEN, CEA, CNRS, CIMAP, 14000 Caen, France*
[c] *Synchrotron SOLEIL, L'Orme des Merisiers, St Aubin, BP 48, 91192 Gif sur Yvette Cedex, France*
[d] *J. Heyrovsky Institute of Physical Chemistry v.v.i., The Czech Academy of Sciences, Dolejskova 3, 18223 Prague, Czech Republic*
[e] *Centro de Computación Científica, Universidad Autónoma de Madrid, 28049 Madrid, Spain*
[f] *Faculty of Exact and Natural Sciences, Siedlce University of Natural Sciences and Humanities, 3 Maja 54, 08-110 Siedlce, Poland*
[g] *Instituto Madrileño de Estudios Avanzados en Nanociencia (IMDEA-Nano), Campus de Cantoblanco, 28049 Madrid, Spain*
[h] *Institute for Advanced Research in Chemical Sciences (IAdChem), Universidad Autónoma de Madrid, 28049 Madrid. Spain*
[i] *Condensed Matter Physics Center (IFIMAC), Universidad Autónoma de Madrid, 28049 Madrid. Spain*
E-mail: patrick.rousseau@unicaen.fr
E-mail: sergio.diaztendero@uam.es

† Electronic Supplementary Information (ESI) available: Geometries of the neutral conformers and statistics of the molecular dynamics for $N-$Methylglycine and $N,N-$Dimethylglycine. See DOI: 10.1039/cXCP00000x/

In this context, the development of biocompatible substances with a protective action against the damaging effects of ionising radiation[24–26] has emerged as a very prominent area of research[27]. In particular, amino acid derivatives[28] and peptides[29] have been proposed as possible radioprotective agents.

It is worth noting that some amino acids such as aromatic, hydrophobic, acidic, or basic amino acids can exert antioxidant activity (see e.g.[30–35]), and the mechanisms in which amino acids and peptides act as radical scavengers are well known[36–38]. In this work, we have joined experimental and theoretical efforts, to study amino acid derivatives with the aim to analyse the possible protective effect that $N-$methylation could have against ionising radiation. $N-$methylation of peptides and proteins is a widely used chemical strategy to enhance its biological functions[39–43]. For instance, it can be used to improve peptide drug properties, since peptides that contain $N-$methylamino acids show higher stability against proteolytic degradation, i.e. degradation by hydrolysis by the action of proteases[44,45]. Another interesting aspect of $N-$methylation is to investigate its potential protective action against ionizing radiation, as it is the case, e.g., of aminothiols[46] and sulfhydryl-containing amino acids[28], especially thiols such as cysteine[47,48] or glutathione[49,50].In particular we study the fragmentation dynamics of two amino acid derivatives after interaction with highly-charged atomic ions in the gas phase: (i) $N-$methylglycine (sarcosine or SMG), an amino acid derivative that was identified in Miller's and Kvenvolden studies and is naturally found in body tissues, and (ii) $N,N-$dimethylglycine (DMG), also present in the human body as a by-product of the metabolic transformation of choline into glycine[51]. The combination of theoretical simulations and experimental measurements yields complementary and more detailed information on the fragmentation dynamics. Thus, theoretical modelling, through *ab initio* molecular dynamics and exploration of the potential energy surface, allows us to obtain information that would be inaccessible from the experiments, such as the molecular mechanisms taking place at the first femtoseconds after ionisation, or the fragmentation pathways leading to the measured fragments. On the other hand, experiments can be used as a reference to test the quality of the simulations and, if required, adapt them to improve their accuracy.

In this work we have found that single $N-$methylation of glycine leads to a much larger variety of fragmentation pathways than non-methylated glycine, while double $N-$methylation effectively closes many of these fragmentation channels, including some of those present in pristine glycine. Importantly, the closure of fragmentation channels in the latter case does not imply a protective effect by the methyl group. In the case of singly $N-$methylated glycine (sarcosine), we observe several channels: the expected Coulomb explosion channel leading to the breakup of the $C_\alpha$-$C_{carboxyl}$ bond; single and double hydrogen transfer; the release of neutral molecules such as CO, $H_2$ or $H_2O$; hydroxyl-group migration, identified as one of the main factors responsible for radiation damage[52]; and the release of radical moieties as methyl groups, also reported as a damaging agent to human health[53]. In the case of doubly $N-$methylated glycine (DMG), we mainly observe Coulomb explosion, typically followed by the loss of neutral stable molecules, and in a few cases molecular reorganisation before cleavage also occurs.

## 2 Methods

### 2.1 Experimental details

The experiments have been performed at the low-energy ion beam facility ARIBE[54] of GANIL in Caen, France. The experimental setup has been described in detail elsewhere[55], only a brief description is given here. A low-energy ion beam (48 keV, $O^{6+}$) has been produced by an electron cyclotron resonance ion source, then mass selected, pulsed, collimated and transported through different optical elements to the interaction zone. Here, it is cross-collided with a beam of neutral amino acid molecules, produced by evaporation of a commercial powder in a heated oven device at 370 K for sarcosine and 329 K for DMG. The cationic products of the interaction between $O^{6+}$ ions and isolated sarcosine and DMG molecules in the gas phase have been studied by means of coincidence time-of-flight (TOF) mass spectrometry using a Wiley-McLaren linear time-of-flight mass spectrometer[21].

At the end of the free-flight region of the spectrometer, all these products were accelerated towards a conversion plate, producing secondary electrons. These electrons were detected by a microchannel plate detector, after being deflected by a weak magnetic field produced by Helmholtz coils. This Daly-type detector allowed efficient and uniform detection of the interaction products over a large mass range. The arrival times were measured in an event-by-event mode. Each event has been characterised by the number of detected fragments and their associated time-of-flights. This allowed us to consider the correlation between the charged fragments proceeding from a single ion–molecule interaction.

In the present experiment with a keV multiply charged ion beam, the dominant process is electron capture by the projectile where at least one electron of the target molecule is transferred to the incoming projectile. In order to get information about the initial charge state of the fragmented target molecule, we analyse the mass spectra associated with nSTOP events. The 1 STOP mass spectrum is created from events where only one charged fragment has been detected after the collision. This mass spectrum illustrates the fragmentation of singly-charged molecules. The 2 STOP mass spectrum is associated with events where two charged fragments were produced in the dissociation of doubly charged molecules and detected in coincidence.

### 2.2 Computational details

Quantum chemistry calculations have been carried out in the framework of the density functional theory (DFT), in particular using the B3LYP functional[56–58], which combines the Becke's three parameter non-local hybrid exchange potential with the non-local correlation functional of Lee, Yang and Parr and the Pople basis set 6-311++G(d,p)[59,60]. Once all conformers were obtained, *ab initio* molecular dynamics were performed using the atom-centered Density Matrix Propagation (ADMP) method[61–63]. ADMP is an extended Lagrangian molecular dynamics method that employs atom-centered Gaussian basis functions and den-

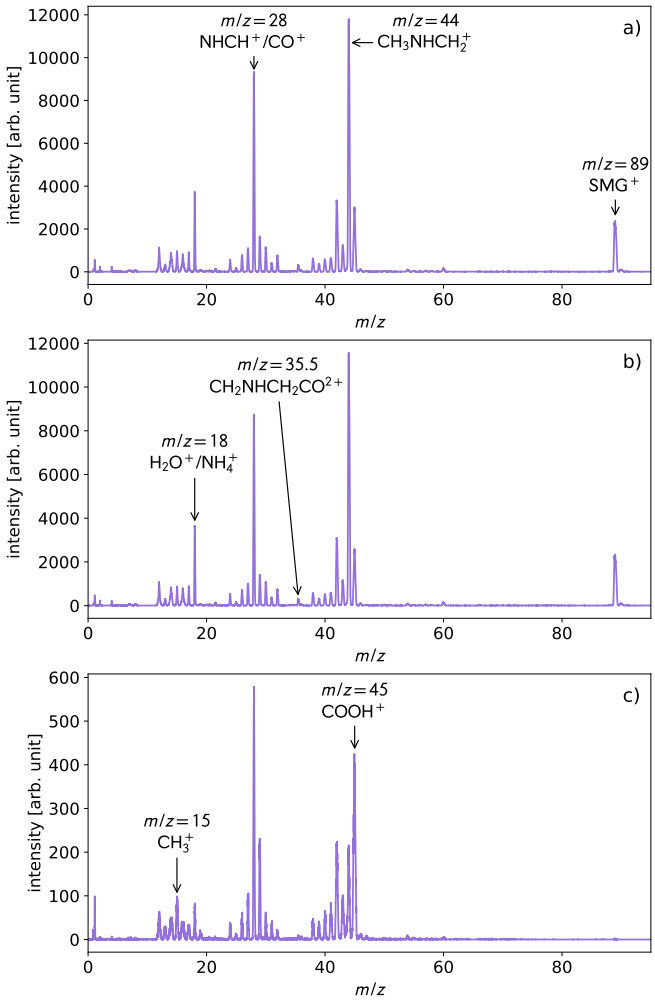


Fig. 1 Experimental mass spectra for sarcosine (SMG) (a) all events, (b) 1-STOP events, (c) 2-STOPS events.

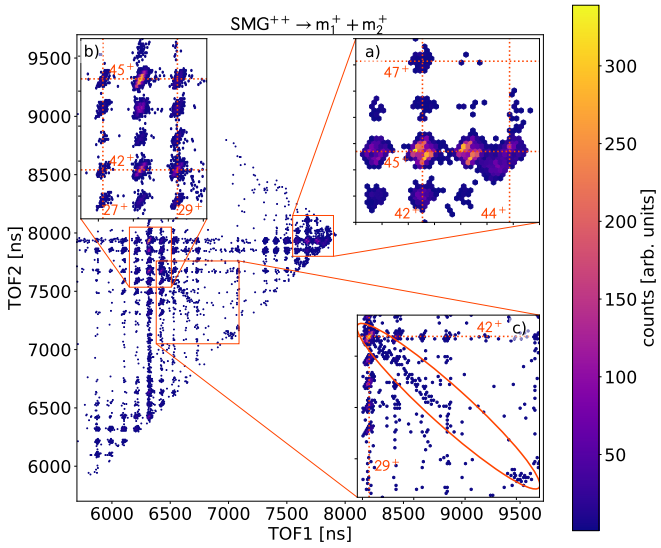


Fig. 2 Experimental 2D coincidence mass spectra of sarcosine. Zooms: (a) coincidence island between fragments ranging from $m_1/z_1 = 42$ to 44, and fragments from $m_2/z_2 = 45$ to 47. Island 44/45 corresponds to path **a**, and island 42/25 to path **b** (see Fig. 4). (b) coincidence islands between fragments ranging from $m_1/z_1 = 27$ to 29, and fragments from $m_2/z_2 = 41$ to 45. (c) delayed fragmentation of the doubly charged fragment $71^{2+}$ giving the fragment ion pair 29+/42+ with the visible tail ending at the expected TOF of the $71^{2+}$ fragment.

sity matrix propagation. In this method the Euler-Lagrange equations of motion for the nuclei and density matrix are integrated, using the velocity Verlet algorithm, thus obtaining the propagation of the nuclei. All trajectories have been carried out using the same functional with the 6-311+G(d,p) basis set. All simulations were performed using a time step of $\Delta t = 0.1$ fs and a fictitious mass of $\mu = 0.1$ amu, to ensure adiabaticity in the dynamics. We have considered a maximum simulation time of $t_{max}$ = 200 fs. To mimic the experimental conditions, we have introduced a certain amount of excitation energy: 5 values between $E_{exc} \approx 0.03$ - 5.44 eV. This range of excitation energy corresponds to the typical transferred energy in ion-molecule collisions[64–72]. We extracted the two electrons from the highest occupied molecular orbital (HOMO) in a Franck-Condon type transition. For each conformer and each value of the excitation energy, 100 trajectory calculations have been carried out. We have selected the 10 most stables conformers of sarcosine, and 6 for DMG. Thus, a total of 5000 trajectories were run for sarcosine and 3000 for DMG. Later on, statistics were performed over these trajectories. On the other hand, sequential dissociation processes, beyond the few hundred fs considered in the *ab initio* molecular dynamics, may play an important role in the fragmentation of the produced molecular ions. Therefore, from the most populated channels observed in the dynamics, we have explored the potential energy surface (intermediate minima and transition states) leading to the fragmentation pathways. Once the transition states for the different reaction paths were obtained, intrinsic reaction coordinate (IRC) calculations were carried out to verify the minima they connect. The combination of *ab initio* molecular dynamics with potential energy surface explorations is very well described in the literature and, nowadays, it has proven to be an effective tool for the study of doubly-charged ions, finding accurate predictions for the experiments[4,22,52]. All calculations were performed by using the Gaussian09 program[73].

## 3 Results and discussion

### 3.1 Stability and fragmentation of doubly ionised sarcosine

Charged fragments generated after interaction of 48 keV $O^{6+}$ ions with sarcosine molecules ($CH_3NHCH_2COOH$) are shown in the so-called inclusive spectrum in Figure 1a, which contains signals from all collision events. It shows an intense signal associated with the singly-charged precursor at $m/z = 89$. However, fragments with smaller $m/z$ values dominate the spectrum. The most intense peak appears at $m/z = 44$, followed by the one at $m/z = 28$. Other interesting peaks appear at $m/z = 45$, and $m/z = 42$. All of them will be discussed further below. Also, a signal at $m/z = 18$ is detected, which might correspond to $H_2O^+$ or $NH_4^+$. More details are obtained by analysing separately the 1-STOP and the 2-STOPS mass spectra (Figure 1b and Figure 1c). These spectra include processes where 1 or 2 charged fragments are produced in a sin-

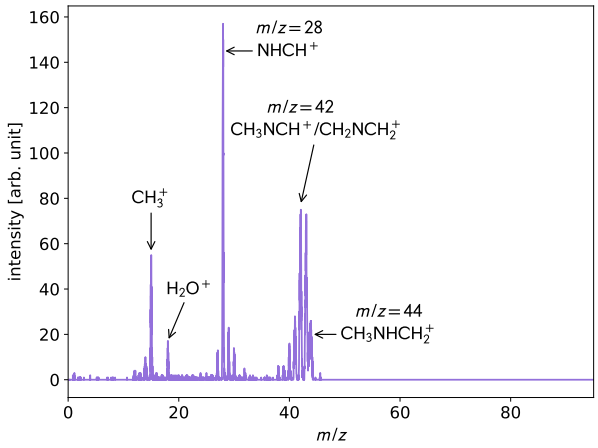


Fig. 3 Experimental mass spectra of sarcosine corresponding to the fragments detected in coincidence with the peak at $m/z = 45$.

gle collision event, respectively. Notice that the 1-STOP spectrum is very similar to the inclusive ion spectrum shown in panel (a) indicating that the production of two charged fragments is much less likely than the production of one charged fragment.

In the 1-STOP spectrum we observe that after $C_\alpha - C_{carboxylic}$ bond cleavage of the singly-charged precursor, the positive charge is localised around the nitrogen atom, leading to a dominant peak at $m/z = 44$ assigned to the $CH_3NHCH_2^+$ fragment. A quite intense peak is also observed at $m/z = 28$. This can be assigned to $NHCH^+$, resulting from further decay of $CH_3NHCH_2^+$ ($m/z = 44$) by the loss of a neutral $CH_4$ molecule. In the case of the 2-STOPS spectrum (Fig. 1c), which originates mainly from the decay of doubly-charged sarcosine ions forming two singly-charged fragments, the relative peak intensities change. Now the peak at $m/z = 28$ becomes dominant followed by the one at $m/z = 45$ which is more intense that the one at $m/z = 44$. As mentioned before, the ion with $m/z = 28$ may result from the emission of $CH_4$ from the fragment with $m/z = 44$. The removal of two electrons by successive electron captures requires a smaller distance of approach ans thus is associated with higher energy deposit. Therefore one can expect an increased dissociation of $CH_3NHCH_2^+$ towards $NHCH^+$ explaining the dominance of $m/z = 28$ fragments in 2-STOPS spectrum. In addition, OH-loss from the fragment $COOH^+$, with $m/z = 45$ may also contribute to the signal at $m/z = 28$ with formation of $CO^+$ ion, although to a smaller extent as detailed below. Other peaks in the 2-STOPS spectrum include the one at $m/z = 29$, which can be attributed to either $COH^+$ or $CH_2NH^+$ fragments, and that at $m/z = 42$, assigned to $CH_3NCH^+$. This last fragment can evolve and, after the loss of hydrogen (either atomic H or molecular $H_2$), leads to $NC_2H_n^+$ ($n = 3-0$), with $m/z = 41-38$. A weak signal at $m/z = 35.5$ can be also appreciated in the 2-STOPS events spectrum, Fig.1c. This would suggest the evolution of a triply charged sarcosine ion leading to the release of the doubly charged $71^{2+}$ fragment in coincidence with other charged fragment. The formation of triply charged ions has been previously observed in collisions of highly-charged ions with other amino acids[22]. Nevertheless, the formation probability of triply charged species is very small, compared to that of doubly and singly charged ions[21].

From the 2 STOP mass spectrum we can plot a coincidence map which shows the correlation between the two detected charged fragments. It is given in Figure 2, where we show the coincidence map for fragmentation of dicationic sarcosine ions leading to the formation of two singly charged fragments. Each event with 2 stops is represented in the map by the time-of-flight of the second fragment ion (TOF2) versus the time-of-flight of the first one (TOF1), thus forming the so-called islands. The coincidence island 44+/45+ is one of the most intense ones and is assigned to Coulomb repulsion after the direct cleavage of the $C_\alpha - C_{carboxylic}$ bond. This rupture leads to two fragments, $COOH^+$ ($m/z = 45$) and $CH_3NHCH_2^+$ ($m/z = 44$). In addition, other intense coincidence islands are observed involving the fragment at $m/z = 45$ along with fragments of smaller $m/z$ values (see Figures 2c and 3). Therefore, we can infer that the $COOH^+$ fragment arrives intact at the detector while the other fragment $CH_3NHCH_2^+$ suffers further dissociation before the detection, as discussed above. However, direct bond cleavage of sarcosine cannot explain all islands observed in the correlation map. Hence, quantum mechanical calculations, in particular ADMP *ab initio* molecular dynamics simulations, have been performed in order to explain the underlying fragmentation mechanisms.

We first performed a conformational study of the neutral sarcosine molecule. Sarcosine is reported to have 13 different conformers[74–77]. Due to the high geometrical similarity between some of them, and in order to optimise the available computational resources, we have selected the ten most stable structures (see ESI: molecules **S1 – S10** in Figure S1). Using these geometries as starting points, *ab initio* molecular dynamics calculations have been performed on the doubly-ionised species. We have identified 12 different reaction paths in the simulations (channels a–l), which have been divided into two main groups: (i) Coulomb explosion and (ii) isomerisation. Among these paths we observed a competition among Coulomb repulsion, hydrogen migration (taking place in $\sim 0-30$ fs), hydroxyl group migration ($\sim 120$ fs) and release of diverse neutral molecules of interest, like carbon monoxide or water. Statistics of the simulations are given in the ESI (see Figure S2). Using the density-functional theory we were able to locate minima and transition states in the potential energy surface, and thus obtain the most favorable structure and fragmentation pathways. This allowed us to build a global picture that explains the most relevant events taking place after excitation and ionisation. The mechanisms and paths obtained in the simulations, explaining the measured fragments in the experiments, are detailed as follows. We have used the following nomenclature: Reaction channels identified in the ADMP simulations are labelled with letters. Since the further fragmentation from the Coulomb Explosion implies a big number of pathways, each one has been labelled with a number.

***$C_\alpha$–$C_{carboxylic}$ bond cleavage:*** Coulomb explosion leading to the $C_\alpha$–$C_{carboxylic}$ bond cleavage (Figure 4 a) distributing the charge between the two fragments $CH_3NHCH_2^+$ and $COOH^+$ ($m/z = 44$ and 45), is the dominant mechanism observed in the

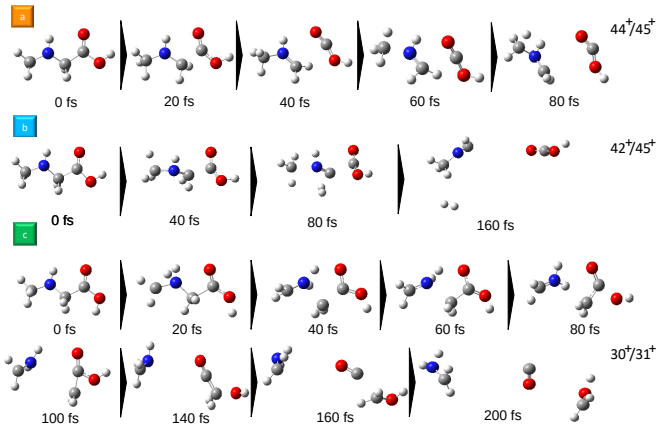


Fig. 4 Snapshots of the molecular dynamics simulations of doubly-charged sarcosine showing the three different fragmentation paths involving as the most relevant event a Coulomb explosion: (a) $C_\alpha$–$C_{carboxylic}$ bond cleavage (b) direct release of neutral $H_2$ followed by $C_\alpha$–$C_{carboxylic}$ bond cleavage (c) OH migration accompanied with molecular fragmentation.

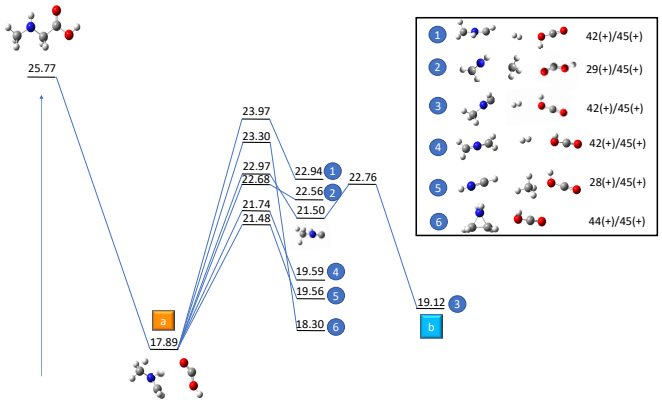


Fig. 5 Stationary points of the potential energy surface (PES) corresponding to fragmentation pathways of the $CH_3NHCH_2^+$ fragment after Coulomb explosion of sarcosine. All energies were calculated at a DFT/B3LYP 6-311++G(d,p) level of theory and are given in eV referred to the most stable neutral sarcosine conformer. This gives the experimentally measured coincidence of one ion with the fragment with $m/z = 45$ a.u., as shown in Fig. 3.

molecular dynamics simulations, especially at lower excitation energies ($\sim 0.03 - 1.36$ eV). In six of the ten conformers, namely **S1**, **S2**, **S4**, **S7** and **S8**, this is the only observed path for all considered excitation energy values. In the correlation map (Figure 2) one can observe a very intense island at 44+/45+, corresponding to the $C_\alpha$–$C_{carboxylic}$ bond cleavage:

$$CH_3NHCH_2COOH^{2+} \rightarrow CH_3NHCH_2^+ + COOH^+, \qquad (1)$$

In the experiments this is one of the most intense islands.

On the other hand, we can see other islands where the peak $m/z = 45$ ($COOH^+$) is in correlation with other species (see also Figure 3). The origin of these islands is found in the subsequent dissociation of the $CH_3NHCH_2^+$ fragment, occurring most probably after the first 300 fs, and therefore not observed in the molecular dynamics calculations. These processes are able to explain

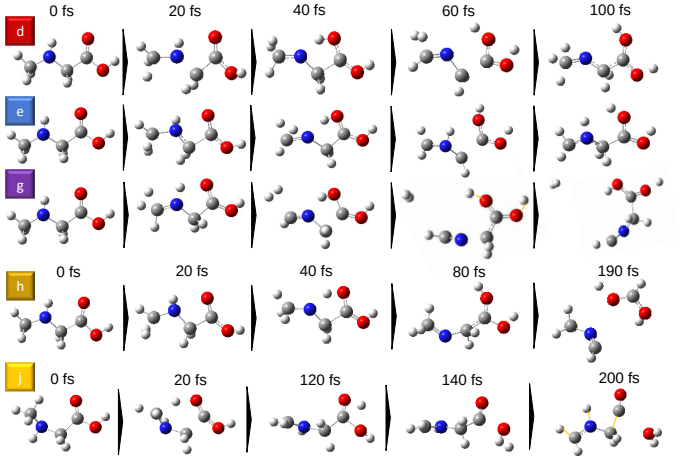


Fig. 6 Snapshots of the molecular dynamics simulations of doubly-charged sarcosine showing the five different fragmentation paths involving an ultrafast hydrogen migration from the amine to the ketonic oxygen as the most relevant event.

signals like 42+/45+, assigned to the release of neutral $H_2$, and leading to the charged fragments $CH_2NCH_2^+$ and $COOH^+$:

$$CH_3NHCH_2^+ + COOH^+ \rightarrow CH_2NCH_2^+ + H_2 + COOH^+ \qquad (2)$$

The neighbor coincidence signal 43+/45+, with also quite high intensity (see Fig. 3), corresponds to the loss atomic hydrogen from the fragment associated to peak 44+, most probably from the N atom. Other fragmentation paths can also lead to the loss of neutral $CH_4$, explaining the highlighted signal at 28+/45+, assigned to $HNCH^+$ / $COOH^+$:

$$COOH^+ + CH_3NHCH_2^+ \rightarrow COOH^+ + NHCH^+ + CH_4 \qquad (3)$$

A third possibility is the direct release of radical methyl $\cdot CH_3$, leading to a significant signal 29+/45+ in the correlation map:

$$COOH^+ + CH_3NHCH_2^+ \rightarrow COOH^+ + NHCH_2^+ + \cdot CH_3 \qquad (4)$$

The stationary points (minima and transition states) in the potential energy surface corresponding to these pathways have been located and are presented in Figure 5.

The methyl radical seems to be involved in carcinogenesis[53], since the hypermethylation of promoter regions of certain genes has been observed in human cancer[78,79]. We have also noticed that, as sarcosine and $\beta$-alanine are structural conformers, resulting fragments of the $C_\alpha - C_{carboxylic}$ bond cleavage are equivalent[23]. Similar to the case of $\beta$-alanine, fragmentation of the doubly-ionised sarcosine can also lead to the formation of charged ethylenimide, a cationic 3-membered ring ($CH_2NH_2CH_2^+$) also proposed as a cell damaging agent, since it has been reported to cause degradation of DNA[80] and, in reaction with 2-desoxy-D-ribose, produces $H_2O_2$[81], a well known strong oxidative compound. Thus, the fragmentation pathways involving the $C_\alpha$–$C_{carboxylic}$ bond cleavage by electrostatic forces, comprise the emission of diverse neutral innocuous molecules, such as $CH_4$ or $H_2$, but also compounds like radical $\cdot CH_3$ or singly-

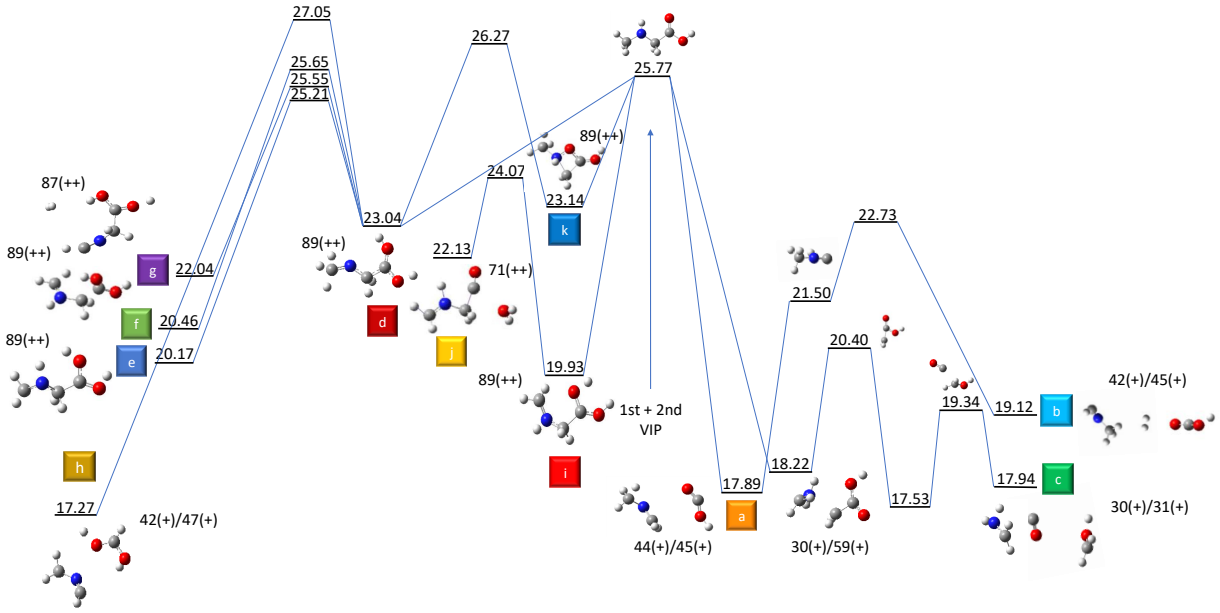


Fig. 7 Potential energy surface of all observed exit channels of doubly positively charged sarcosine. All energies were calculated at a DFT/B3LYP 6-311++G(d,p) level of theory and are given in eV referred to the most stable neutral sarcosine conformer. Labels correspond to the trajectories in the molecular dynamics simulations – see Figs. 4 and 6

charged ethylenimide. The latter two have been proposed as detrimental for human health and all produced with a relatively strong intensity in the fragmentation of dication sarcosine. However, while the $CH_3NHCH_2^+$ fragment is exposed to further fragmentation, shown in Figure 5, other mechanisms corresponding to further fragmentation of the $COOH^+$ appear at much higher energy[19], thus contributing in much lower percentage in the correlation map.

***Direct release of neutral $H_2$:*** In this case, the two hydrogens from the methylene group are released as molecular $H_2$ in a concerted mechanism with a subsequent Coulomb repulsion leading to the $C_\alpha - C_{carboxylic}$ bond cleavage (see Figure 4b). This exit channel produces the cationic molecular fragments $CH_3NHC^+$ and $COOH^+$, corresponding to the coincidence signal 42+/45+, one of the most intense islands in this spectrum.

$$CH_3NHCH_2COOH^{2+} \rightarrow COOH^+ + CH_3NCH^+ + H_2 \qquad (5)$$

After the release of both methylene hydrogens, an ultrafast H transfer takes place from $CH_3NHC^+$ to $CH_3NCH^+$; Figure 7 shows the corresponding energy path.

At lower energies, the simulations show, in agreement with the experiment, that Coulomb explosion is the dominant process. At higher energies, other pathways like hydrogen migration show up. These reactions depend strongly on the molecular structure. Similar conformers are more likely to present similar isomerisations, as in the case of **S3** and **S9**, where the first hydrogen migration occurs in a similar way. The simulations describe also mechanisms responsible for very low-intensity signals in the experimental spectra, as for example the fragmentation product of pathway **j** in Figure 7, which explains the peak in the 1-STOP spectrum at $m/z = 35.5$, formed after the release of neutral $H_2O$.

Some alternative reaction paths are in competition with Coulomb explosion. They involve ultrafast H migration ($\sim 30-40$ fs) as a first step, followed by other possible paths. In addition, these isomerisations are also of high relevance for subsequent reaction and fragmentation paths, arriving in some cases to the emission of neutral molecules such as $H_2$, CO or $H_2O$. Ultrafast double hydrogen migration has been recently reported in ethanol[82] and in acetonitrile[83].

***H migration from the amine to the carbonyl oxygen:*** Among the pathways involving hydrogen migration as a first step, the one exhibiting H transfer from the amine to the carboxylic oxygen of the acid is statistically the most relevant one. For example, in the third most stable conformer, **S3**, $\sim 18\%$ of the total number of trajectories involve this migration. This reaction path is observed as well for conformer **S9**. Both isomers (**S3** and **S9**) share a linear structure and a similar relative position between the carbonyl and the amine groups, leading to a similar interaction between them. Five different reaction paths are found starting with H migration from the amine to the ketonic oxygen (see Fig. 6). Channel **d** corresponds to those trajectories in which a doubly-charged geminal diol is stabilized (within the limited propagation time considered in the calculations, it does not lead to further fragmentation):

$$CH_3NHCH_2COOH^{2+} \rightarrow CH_3NCH_2C(OH)_2^{2+} \qquad (6)$$

In channel **e**, together with the first H migration, a second one takes place from the terminal methyl to the amine in a concerted mechanism; i.e. a double H migration also stabilizes a geminal diol:

$$CH_3NHCH_2COOH^{2+} \rightarrow CH_2NHCH_2C(OH)_2^{2+} \qquad (7)$$

A third group of trajectories also includes a second hydrogen migration between the methylene and the amine's nitrogen, which

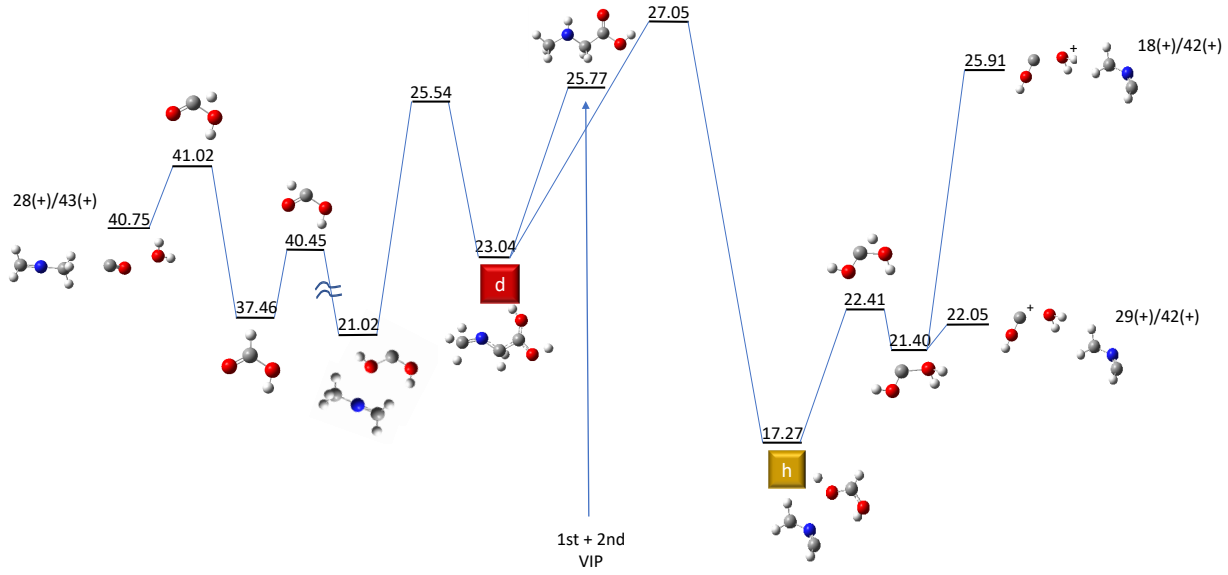


Fig. 8 Potential Energy Surface exploration of the fragmentation pathways for doubly positively charged sarcosine. We include two different possible fragmentation pathways starting from the isomer created after the N → O hydrogen migration that leads to the formation of neutral or charged $H_2O$, CO or COH. All energies were calculated at a DFT/B3LYP 6-311++G(d,p) level of theory and are given in eV referred to the most stable neutral conformer.

is slower than the first one (it takes place in $\sim 100-120$ fs):

$$CH_3NHCH_2COOH^{2+} \rightarrow CH_3NHCHC(OH)_2^{2+} \quad (8)$$

The forth and the fifth exit channels present multi-step character showing combined processes in the same trajectory. Path **g** implies emission of neutral $H_2$ after the H migration leading to a doubly charged fragment ($m/z = 43.5$):

$$CH_3NHCH_2COOH^{2+} \rightarrow CHNCH_2C(OH)_2^{2+} + H_2 \quad (9)$$

In **h**, after the ultrafast migration of the first hydrogen, a second hydrogen migration takes place between the methylene and the carboxylic carbon and immediately thereafter, the $C_\alpha$–$C_{carboxylic}$ bond breaks into two singly-charged fragments ($m/z = 42/47$):

$$CH_3NHCH_2COOH^{2+} \rightarrow CH_3NCH^+ + CH(OH)_2^+. \quad (10)$$

The statistical analysis (see Figure S2 in the ESI) shows that the reaction path **g** has a higher relevance. In fact, for conformer **S3**, $\sim 10\%$ of the total trajectories follow this path and in the case of the **S9** $\sim 2\%$. The energy barrier leading to **g** is very high and, accordingly, only relevant at the highest excitation energies in the dynamics, which explains the very small abundance extracted by the 1-STOP spectrum. The doubly-charged precursor molecule gives a signal at $m/z = 44.5$ in the mass spectrum, while the doubly-charged fragment after emission of neutral $H_2$ does at $m/z = 43.5$. This is an $m/z$ range in the spectra with dominant peaks associated with Coulomb explosion and we can hardly infer the presence of these species. Indeed, the peak at 43.5 is somewhat masked by the high intensity of the surrounding peaks but it seems that a weak signal can be attributed to this fragment, and therefore to those channels with $H_2$ emission after H transfer, confirming the occurrence of such mechanism.

The highest stability of the exit channel of path **h** appears to be of particular interest. However it should be taken into consideration that the transition state connecting **d** with **h** lies at higher energy than the initial vertical ionisation potential. Therefore, even though very stable, this path is kinetically hindered by such a big energetic barrier; only excitation energies larger than $\sim 2$eV would overcome the barrier. The low intensity of the 42+/47+ island (Fig. 2) confirms this theoretical prediction.

***H migration from the methyl to the carbonyl oxygen:*** The structure of conformer **S6** allows for a direct interaction between the carbonyl oxygen of the carboxylic acid and the methyl group. This favours an ultrafast hydrogen transfer from the latter to form a geminal diol. The reaction pathway takes place during the first $\sim 30$ fs of the simulations. Afterwards, the molecule is stabilised (see channel **i** in Fig. 7):

$$CH_3NHCH_2COOH^{2+} \rightarrow CH_2NHCH_2C(OH)_2^{2+} \quad (11)$$

or undergoes a second hydrogen migration from one hydroxyl of the diol to the other leading to the emission of neutral water (channel **j**):

$$CH_3NHCH_2COOH^{2+} \rightarrow CH_2NHCH_2CO^{2+} + H_2O \quad (12)$$

The left part of (Fig. 7) shows the most relevant points of the potential energy surface implying such H migration. Minima corresponding to diol stabilisation and transition states of paths leading to neutral $H_2$ and $H_2O$ emission are shown. The peak at $m/z = 35.5$ confirms the neutral water release from doubly-charged sarcosine.

The right part of Fig. 8 shows further evolution of the $CH(OH)_2^+$ fragment formed in channel **h** . The potential energy surface exploration shows that it can evolve through H migration from one of the hydroxyl groups to the other, with final emission of

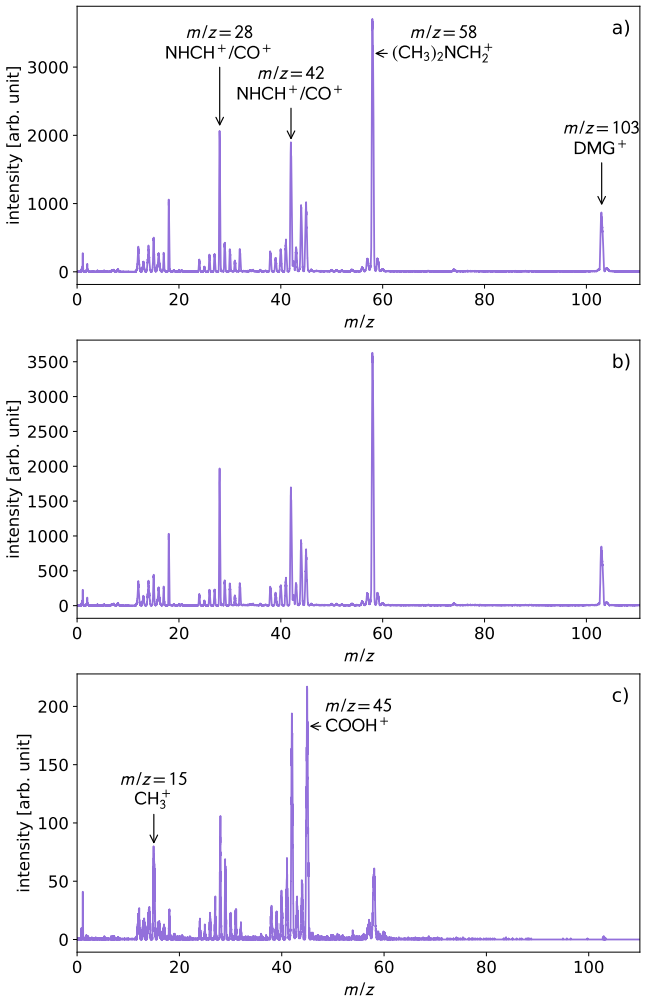


Fig. 9 Experimental mass spectra of $N,N-$dimethylglycine (a) all events, (b) 1-STOP events, (c) 2-STOPS events.

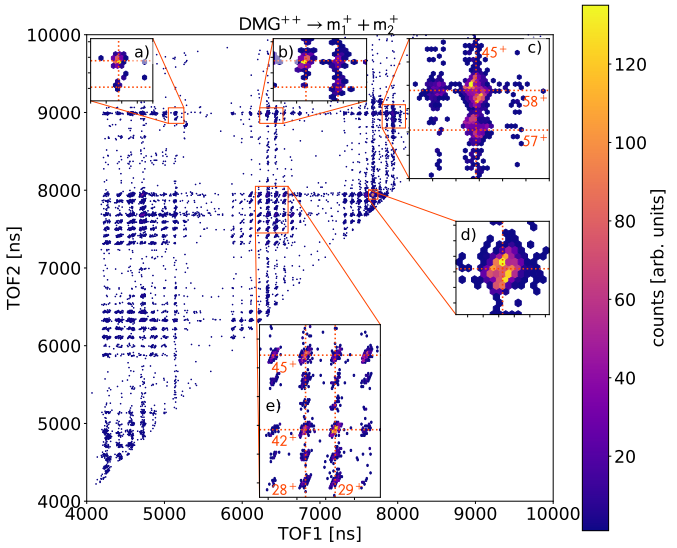


Fig. 10 Experimental 2D coincidence mass spectra of $N,N-$dimethylglycine. Zooms: (a) Coincidence islands between fragments with $m/z = 17,18$ and $m/z = 58$. (b) Coincidence islands between fragments with $m/z = 28,29$ and $m/z = 58$. (c) Coincidence islands between fragments with $m/z = 44,45$ and $m/z = 57,58$. Island 45/58 corresponds to path **a** (see Fig. 12). (d) Coincidence island between fragment with $m/z = 42$ and $m/z = 45$. (e) Coincidence islands between fragments with $m/z$ ranging from 27 to 30, and fragments from $m/z = 40$ to 45.

neutral or singly-charged water (being the second one much less favourable energetically):

$$CH_3NCH^+ + CH(OH)_2^+ \rightarrow CH_3NCH^+ + COH^+ + H_2O \quad (13)$$

$$\rightarrow CH_3NCH^+ + COH + H_2O^+ \quad (14)$$

The first channel, producing fragments $CH_3NCH^+$, $COH^+$ and $H_2O$, is found in the coincidence map signal at 29+/42+. This island has been indeed observed with relatively high intensity and, at the same time, presents a long tail (see coincidence 29+/42+ associated with the tail of the $71^{2+}$ fragmentation in Fig. 2c), which is the typical signature of a delayed fragmentation. The time-of-flight spectrometer employed in this work is able to detect the fragmentation of meta-stable ions on a microsecond time scale. In this case, the metastable decomposition reaction is assigned to the loss of neutral water: after ultrafast H migration leading to a stable diol (structure **d** in Fig. 8), a high energetic barrier should be reached towards production of $CH_3NCH^+ + CH(OH)_2^+$ (transition state at 27.05 eV – pathway **h** in Figure 8), with a further emission of neutral $H_2O$. The kinetically unfavourable reaction due to the high barrier leads to a metastable situation in which the emission of the recorded fragments takes place in a microsecond timescale, thus explaining the tail in the spectra. We observed a similar metastable decomposition of the N-acetylglycine cation, where a tautomerisation enabled by the peptide bond produced delayed fragmentation[84].

***OH migration:*** In this group we found two exit channels, both observed in the molecular dynamics simulations. In the first one, an ultrafast H migration from the methyl to the amine nitrogen is followed by Coulomb explosion, breaking the $C_\alpha$–$C_N$ bond, and leading to $CH_2NH_2^+ + CH_2COOH^+$. In the second channel, the system further evolves through an OH migration from the $C_{carboxylic}$ to the $CH_2$ leading to the emission of neutral CO (see in Figure 4c snapshots of one example trajectory producing this path):

$$CH_3NHCH_2COOH^{2+} \rightarrow CH_2NH_2^+ + CH_2COOH^+ \rightarrow (15)$$

$$\rightarrow \quad CH_2NH_2^+ + CH_2OH^+ + CO \quad (16)$$

Interestingly, while (15) is almost negligible in the coincidence spectrum, the channel leading to the emission of neutral CO is more relevant. This fact indicates that for longer timescales, the exit channel (15) tends to evolve into (16).

### 3.2 Stability and fragmentation of doubly ionised *N,N*-dimethylglycine

Species formed after the collision of neutral DMG ($(CH_3)_2NCH_2COOH$) with an $O^{6+}$ ion beam at 48 keV have also

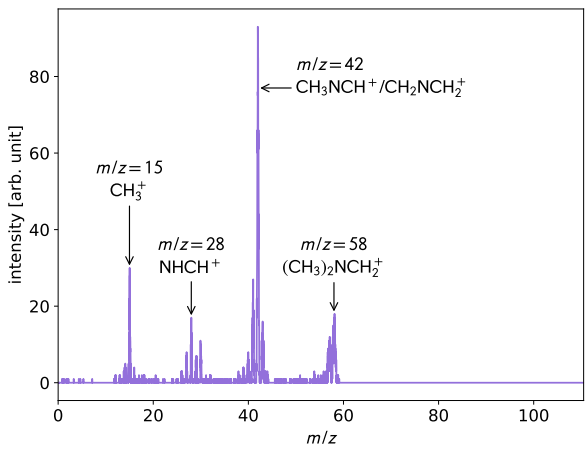


Fig. 11 Experimental mass spectra of $N,N-$dimethylglycine corresponding to the fragments detected in coincidence with the peak at $m/z = 45$.

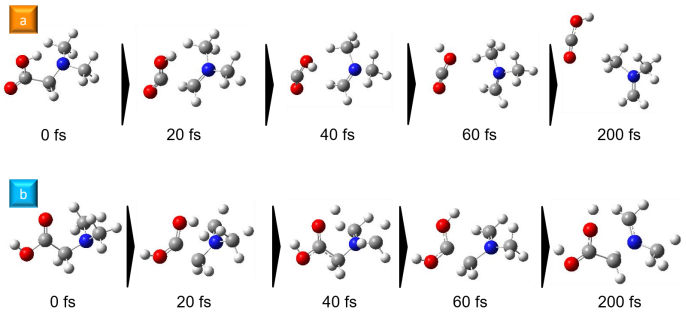


Fig. 12 Snapshots of the molecular dynamics simulations of doubly-charged dimethylglycine showing the two different fragmentation paths observed. (a) $C_\alpha - C_{carboxylic}$ bond cleavage. (b) Ultrafast hydrogen migration.

been measured and analysed (see the most relevant recorded spectra in Figures 9, 10 and 11).

The main peaks in the 1-STOP spectrum are assigned as follows. The most intense peak ($m/z = 58$) corresponds to $CH_2N(CH_3)_2^+$ as a result of the $C_\alpha - C_{carboxylic}$ bond cleavage. The high intensity of this peak shows the preference of the positive charge to be hosted by the amine fragment, as in the case of singly-charged sarcosine. The signal at $m/z = 28$, can be explained by fragmentation processes of the most intense peak, leading to $HNCH^+$. The evolution of $CH_2N(CH_3)_2^+$, obtained through exploration of the potential energy surface, can also explain the detection at $m/z = 42$, if one considers loss of neutral $CH_4$ producing $CH_2NCH_2^+$. Among the most relevant peaks, we also observe that corresponding to the singly-charged precursor, DMG molecule at $m/z = 103$. On the other hand, in the 2-STOPS spectrum, we can also see a signal at $m/z = 45$, most probably corresponding to the $COOH^+$ fragment originated after $C_\alpha - C_{carboxylic}$ bond breaking in a Coulomb explosion processes of the doubly-charged DMG. In this case, the charge is shared by the two generated fragments.

Fig. 10 shows the most important peaks recorded in coincidence. One of the coincidence peaks is, as expected, the one corresponding to the $C_\alpha - C_{carboxylic}$ bond cleavage at 45+/58+. This cleavage is also responsible for other intense peaks due to the following fragmentation of the amine fragment. The signal at 42+/45+ corresponds to the loss of neutral $CH_4$ from the fragment hosting the amino group, leading to $COOH^+/CH_3NCH^+$ or $COOH^+/CH_2NCH_2^+$. Coincidence detection at 28+/45+ can be associated to $HNCH^+/COOH^+$. The last highlighted island at 28+/42+ can be assigned to $CH_2NCH_2^+/CO^+$ or $CH_3NCH^+/CO^+$, considering the fragmentation of the $COOH^+$ fragment.

The experimental results for DMG show a smaller variety of processes leading to fragmentation. To identify all the possible dissociation paths and explain the underlying fragmentation mechanisms, we have also performed molecular dynamics calculations. A first step was a conformational study of the neutral DMG molecule. The addition of an extra methyl group to the amine leads to an effective reduction of degrees of freedom, so, as expected, a smaller number of conformers has been found compared to sarsosine. We have identified six different conformers for the neutral DMG molecule (see Figure S3 in the ESI). For each one, we carried out 100 trajectory calculations using the same 5 values of excitation energy (see ESI). Only two different types of processes are observed in the simulations. The first one corresponds to Coulomb explosion leading to the cleavage of the $C_\alpha - C_{carboxylic}$ bond (see Fig. 12a). The second one, involves an ultrafast H-migration ($\approx 40$ fs) from one of the $N-$methyl groups to the carbonyl oxygen (see Fig. 12b). We detail the corresponding pathways by exploring the potential energy surface of each process separately. We have used the same nomenclature as in the sarcosine case; i.e. letters for the exit channels as identified in the dynamics and numbers for those pathways coming from further fragmentation after Coulomb Explosion.

***Coulomb Explosion***: The excess of charge leads to an electric repulsion that triggers the break-up of the $C_\alpha - C_{carboxylic}$ bond producing two charged fragments, 45+/58+:

$$(CH_3)_2NCH_2COOH^{2+} \rightarrow COOH^+ + (CH_3)_2NCH_2^+ \qquad (17)$$

This fragmentation pathway absolutely dominates the statistics. All the trajectories in four conformers (**DMG1**, **DMG4**, **DMG5** and **DMG6**) follow this pathway, and for the other two conformers (**DMG2** and **DMG3**) it clearly represents the most probable event; For the whole picture of the statistics see Figure S4 in the ESI.

Following this exit channel, we have further explored the fragmentation scheme of the amine part, as it is shown experimentally that it might experience fragmentation after Coulomb explosion. Eleven possible evolution paths are considered: Minima and transition states corresponding to the evolution in these channels can be seen in Fig. 13.

1. The first point in the PES corresponds to the fragmentation products of Coulomb explosion after $C_\alpha - C_{carboxylic}$ bond break (see eq. (17)). After this, the amine fragment starts to fragment and can follow two different paths (2 and 3):

2. The first path does not involve any loss of mass, but an isomerisation: it consists of the torsion of the $C_{methylic} - N -$

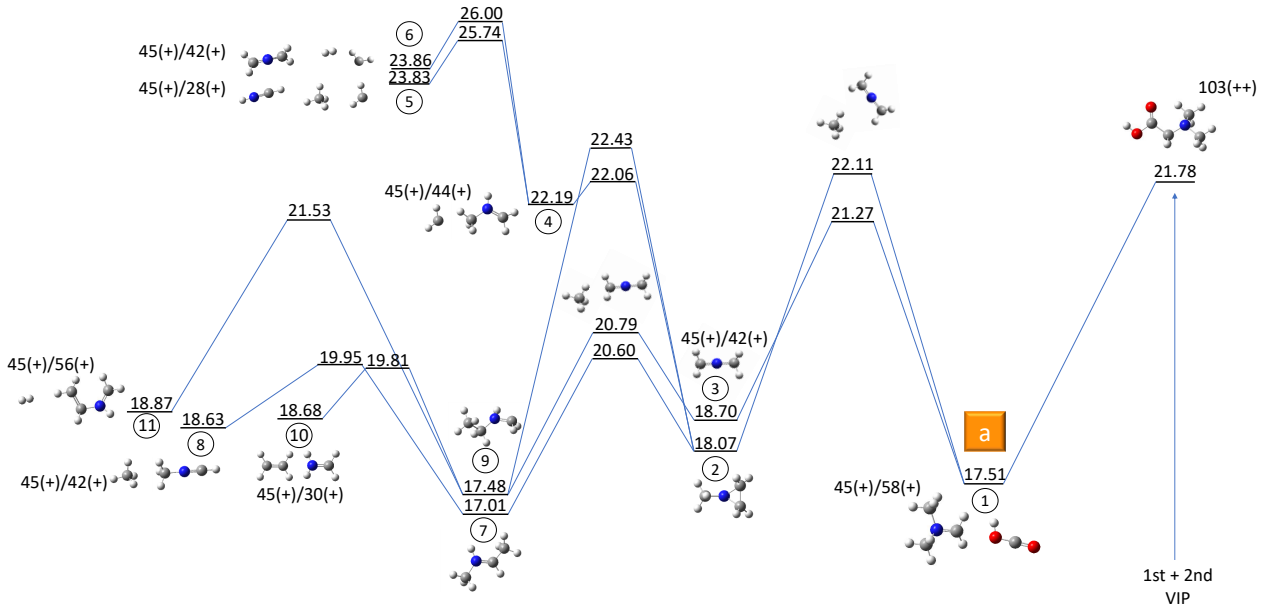


Fig. 13 Potential Energy Surface exploration for the fragmentation pathways of doubly-charged dimethylglycine after Coulomb explosion (channel **a** in the dynamics). All energies were calculated at a DFT/B3LYP 6-311++G(d,p) level of theory and are given in eV referred to the most stable neutral conformer.

$C_{methylenic}$ angle, leading to a 3-membered cycle (labeled as 2 in Fig. 13) with a hydrogen transfer from the methyl involved in the torsion to the nitrogen.

$$(CH_3)_2NCH_2^+ \rightarrow CH_3 - NH \begin{array}{l} \diagup CH_2^{\,+} \\ \diagdown\ CH_2 \end{array} \qquad (18)$$

3. In the second pathway, new fragments are formed involving the loss of neutral $CH_4$ from the amine fragment.

$$(CH_3)_2NCH_2^+ \rightarrow CH_2NCH_2^+ + CH_4 \qquad (19)$$

The release of neutral $CH_4$ entails the hydrogen transfer from one of the methyl groups to the other one, leading to the $CH_2NCH_2^+$ charged fragment recorded in coincidence with $COOH^+$, corresponding to the island at 42+/45+.

4. The cyclic minimum (in path 2) can evolve in three different pathways (4, 7 and 9). In pathway 4 we observe the release of neutral $CH_2$ leading to a fragment with $m/z = 44$:

$$CH_3CH_2NHCH_2^+ \rightarrow CH_3NHCH_2^+ + CH_2 \qquad (20)$$

This path can be followed by subsequent emission of neutral fragments (paths 5 and 6).

5. Release of $CH_4$ from path 4:

$$CH_3NHCH_2^+ \rightarrow HNCH^+ + CH_4 \qquad (21)$$

leading to the coincidence detection 28+/45+, i.e. corresponding to $CHNH^+/COOH^+$ (Fig.10e).

6. Release of $H_2$ from path 4:

$$CH_3NHCH_2^+ \rightarrow CH_2NCH_2^+ + H_2 \qquad (22)$$

corresponding to the signal at 42+/45+; fragments $CH_2NCH_2^+/COOH^+$ (Fig.10d).

7. Other possibility from path 2 consists in the isomerisation of the 3-membered cycle leading to the translocation of one of the $N-$methylenes of the cycle to the other methylene dragging its hydrogen with it (pathway 7):

$$CH_3CH_2NHCH_2^+ \rightarrow CH_3NHCHCH_3^+ \qquad (23)$$

This path would also lead to a signal 45+/58+ (Fig.10c).

8. Evolution from path 7 through the migration of the amine hydrogen to the methylene methyl, leads to the release of neutral $CH_4$:

$$CH_3NHCHCH_3^+ \rightarrow CH_3NCH^+ + CH_4 \qquad (24)$$

that would correspond to the 42+/45+ signal, fragments $CH_3NCH^+/COOH^+$.

9. Interestingly, the third pathway from 2 matches with the pathway that follows 3, through different transition states (being the transition state from 2 at much higher energy than the one from 3). The transposition of the $N-$methyl group to one of the methylene groups forms the cycle labelled as 9 in the figure:

$$CH_3 - NH \begin{array}{l} \diagup CH_2^{\,+} \\ \diagdown\ CH_2 \end{array} \rightarrow CH_3CH_2NHCH_2^+ \qquad (25)$$

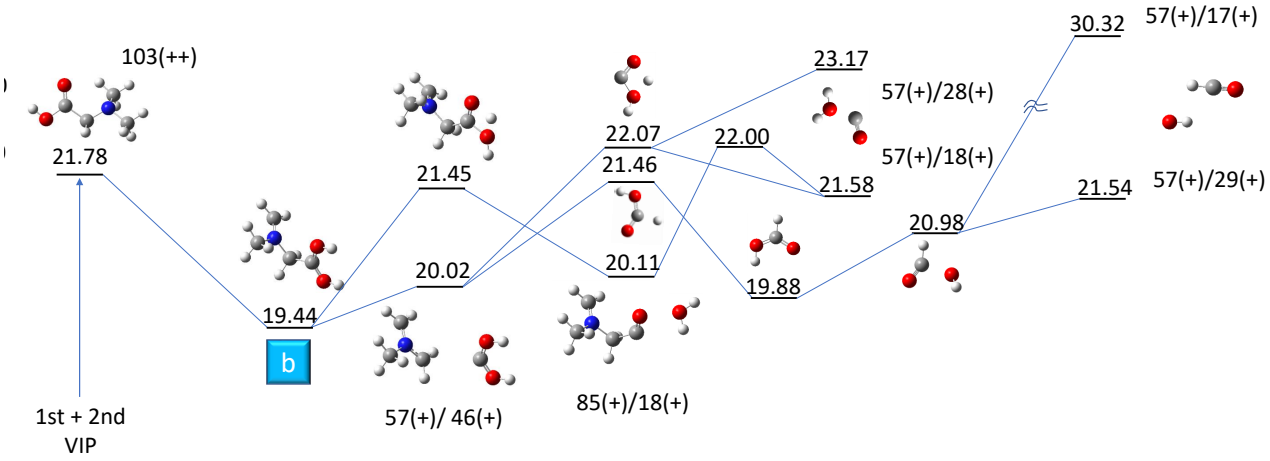


Fig. 14 Fragmentation pathways for the doubly-charged dimethylglycine after the ultrafast hydrogen migration takes place (pathway b). All energies were calculated at a DFT/B3LYP 6-311++G(d,p) level of theory and are given in eV referred to the most stable neutral conformer.

corresponding to the coincidence 45+/58+.

10. Then, from 9 the system could evolve in two different ways, one via hydrogen migration from the methyl to the amine that triggers the dissociation of the molecule leading to the release of neutral ethylene $CH_2=CH_2$ (pathway 10):

$$CH_3CH_2NHCH_2^+ \rightarrow CH_2NH_2^+ + CH_2CH_2 \qquad (26)$$

Signal 30+/45+ in the spectrum (Fig.10e) , corresponding to fragments $CH_2NH_2^+/COOH^+$

11. And the second path from 9 that consists of the direct release of neutral $H_2$ (pathway 11)

$$CH_3CH_2NHCH_2^+ \rightarrow CH_2CHNHCH_2^+ + H_2 \qquad (27)$$

Signal 45+/56+ in the spectrum, corresponding to fragments $CH_2CHNHCH_2^+/COOH^+$

Fragments in coincidence with the one at $m/z = 45$ are shown in Fig. 11. The different pathways described above explained the observed ion pairs.

One of the most remarkable differences between the fragmentation of DMG in comparison with sarcosine, is the behaviour in the evolution of the fragment in coincidence with $COOH^+$ after Coulomb explosion. While in the case of sarcosine, loss of atomic and molecular hydrogen are shown as quite important, peaks at m/z= 43 and 42 present much higher intensity than that at 44 in Fig. 3, in DMG the equivalent detection signals m/z = 57 and 56 are much smaller than that at 58 in Fig. 11. This points out a clear evidence of the preferential loss of hydrogen from the N atom in sarcosine, obviously not possible in DMG due to the double methylation of the N atom. In stead, in DMG the dominant signal in coincidence with the peak at 45, is that at 42 after the loss of $CH_4$, being by far the dominant coincidence in the experiment (Fig. 10).

***Isomerisation – H migration:*** The only fragmentation pathway that appears in competition with Coulomb explosion is isomerisation of the amino acid via ultrafast hydrogen migration from one of the $N-$methyl groups to the carboxylic oxygen:

$$(CH_3)_2NCH_2COOH^{2+} \rightarrow$$

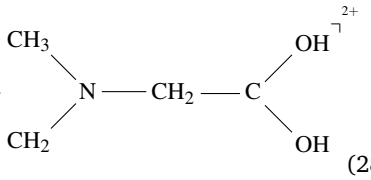


(28)

Figure 14 shows the minima and transition states corresponding to the pathways that follow hydrogen migration. Two possible evolution pathways may take place. The first one is slightly higher in energy and involves a second H migration between the hydroxyl groups leading to the formation of singly charged water followed by the release of neutral CO (a small signal 57+/18+ was detected). The second path has the same nature but before the second hydrogen migration took place the $C_\alpha - C_{carboxylic}$ bond breaks ($57^+/46^+$). This allows the charge to be located either in the CO ($57^+/28^+$), or the $H_2O$ ($57^+/18^+$) after the second H migration takes place. Finally, hydrogen migration from one of the hydroxyl groups to the carbon leads to formation of singly charged $HCO^+$ and neutral OH, explaining the signal 57+/29+. Note that all these islands (18+/57+, 28+/57+ and 29+/57+) are observed in the coincidence map (Fig. 11).

## 4 Concluding remarks

In this work we have presented a joint experimental and theoretical study concerning the fragmentation dynamics of excited doubly ionised $N-$methylglycine (sarcosine) and $N,N-$dimethylglycine (DMG) in the gas phase. Experimental results, obtained through the detection of multicoincidence mass spectroscopic techniques, are interpreted with the help of *ab initio* molecular dynamics (AIMD) simulations and density-functional theory calculations. We have been able to achieve a better understanding of the effects of ionising radiation in these two amino acid derivatives.

The main exit channel when both amino acids are doubly-ionised is the Coulomb explosion, with the $C_\alpha - C_{carboxylic}$ bond cleavage leading to $COOH^+$ and a charged amino fragment.

This behaviour is common to all amino acids previously studied[4,12,19–23]. This result has been confirmed with the molecular dynamics simulations, being the most probable exit channel for both amino acids, and with the exploration of the potential energy surfaces, where the mechanisms leading to these channels show a barrier-less pathway and very stable low-energy minima, also for both amino acids. In the case of sarcosine, several other fragmentation paths have been observed in competition with Coulomb explosion; Among them, hydrogen migration, along with hydroxyl migration and the release of neutral molecules like $H_2O$, $H_2$ and CO. Hydrogen transfer has been suggested to play a role in the dissociation of protonated oligonucleotides[85]. Furthermore, the presence of hydroxyl radicals in biological tissues has been identified as one of the main factors responsible for radiation damage[86–89].

In the case of DMG, only one path has been found to be in competition with Coulomb explosion: an ultrafast hydrogen migration from one of the $N-$methyl groups to the carboxylic oxygen. Analysing these results, it is concluded that the fragments resulting from the evolution of the system after Coulomb explosion dominate the experimental spectra. Thus, the greater variety of mechanisms observed in sarcosine, comes from the richness of its fragmentation in the first femtoseconds after ionization, while for DMG only the degradation of two channels are obtained.

In comparison with sarcosine, the molecular dynamics results show that DMG exhibits less fragmentation pathways, which one could be tempted to explain by a possible protective effect exerted by the extra methyl group at the amine position, limiting the evolution of the system after interaction with the ion beam. To confirm or discard this hypothesis, we can compare these findings with those previously reported for glycine in similar experiments[19]. Our results for the doubly-methylated glycine (DMG) are rather similar to those obtained for doubly-charged glycine, where, in competition with Coulomb explosion, only one alternative path was present, namely an ultrafast hydrogen migration. However, in the case of DMG, H transfer to the amino group is blocked by the double methylation, while in glycine H transfer was observed to happen towards both the carboxylic and the amine groups. When the symmetry is broken by the substitution of just one methyl group, as in sarcosine, a much more colourful palette of fragmentation patters and different migrations appear, which are in fact very similar to those previously reported for the doubly-charged $\beta$-alanine[23], its structural functional isomer. Hence, substitution with methyl groups does not seem to induce any protective effect but rather leads to a larger variety of fragmentation processes , as in the case of single $N-$methylation, or to less fragmentation, as in the case of double $N-$methylation. This result suggests that $N-$methylation might be used to selectively open or close fragmentation pathways that are, respectively, absent or natural in the pristine non methylated compound.

## Author Contributions

D.B.-L., A.L. and S.D.-T. performed the simulations. C.N., J.K., J.K., B.A.H., A.D. and P.R. performed the experiments. All authors were involved in the interpretation of the data. D.B.-L., C.N., P.R. and S.D.-T. wrote the original manuscript. All authors thoroughly reviewed the manuscript and contributed to the final version, suggesting comments for the presentation and discussion of the results. P.R. and S.D.-T. conceived and supervised the project.

## Conflicts of interest

There are no conflicts to declare.

## Acknowledgements

The experiments have been performed at the ARIBE facility, part of large-scale infrastructure GANIL. The Research was conducted in the framework of the International Associated Laboratory (LIA) Fragmentation DYNAmics of complex MOlecular systems - DYNAMO, funded by the Centre National de la Recherche Scientifique (CNRS) and in the frame of the COST action CA18212 - Molecular Dynamics in the GAS phase (MD-GAS). We acknowledge the technical support by J.-M. Ramillon, C. Feierstein and T. Been. The authors acknowledge the generous allocation of computer time at the Centro de Computación Científica at the Universidad Autónoma de Madrid (CCC-UAM). This work was partially supported by the MICINN - Spanish Ministry of Science and Innovation - projects PID2019-110091GB-I00 and PID2019-105458RB-I00 funded by MCIN/AEI/10.13039/501100011033, the 'María de Maeztu' Program for Centers of Excellence in R&D (CEX2018-000805-M) and the 'Severo Ochoa' Programme for Centres of Excellence in R&D (SEV-2016-0686). The work has been partially funded by the project INCa-ITMO (N PC201307) within the Programme Plan Cancer 2009-2013 (Inserm). D.B.-L. acknowledges the FPI grant associated with the project CTQ2016-76061-P. CN is co-funded by Région Normandie and Synchrotron SOLEIL.

## Notes and references

1 S. L. Miller, *Science*, 1953, **117**, 528–529.
2 K. A. Kvenvolden, J. G. Lawless and C. Ponnamperuma, *Proceedings of the National Academy of Sciences*, 1971, **68**, 486–490.
3 G. Munoz-Caro, U. Meierhenrich, W. Schutte, B. Barbier, A. Arcones-Segovia, H. Rosenbauer, W.-P. Thiemann, and J. Brack, A.and Greenberg, *Nature*, 2002, **416**, 403—-406.
4 D. G. Piekarski, R. Delaunay, S. Maclot, L. Adoui, F. Martín, M. Alcamí, B. A. Huber, P. Rousseau, A. Domaracka and S. Díaz-Tendero, *Phys. Chem. Chem. Phys.*, 2015, **17**, 16767–16778.
5 L. Sanche, *The European Physical Journal D - Atomic, Molecular, Optical and Plasma Physics*, 2005, **35**, 367–390.
6 E. Stadtman, *Science*, 1992, **257**, 1220–1224.
7 J. Grotemeyer, U. Boesl, K. Walter and E. W. Schlag, *Journal of the American Chemical Society*, 1986, **108**, 4233–4234.
8 J. Grotemeyer and E. W. Schlag, *Accounts of Chemical Research*, 1989, **22**, 399–406.
9 T. Wyttenbach and M. T. Bowers, *Journal of the American Society for Mass Spectrometry*, 1999, **10**, 9 – 14.
10 J. de Vries, R. Hoekstra, R. Morgenstern and T. Schlathölter, *Phys. Rev. Lett.*, 2003, **91**, 053401.

11 T. Schlathölter, F. Alvarado, S. Bari, A. Lecointre, R. Hoekstra, V. Bernigaud, B. Manil, J. Rangama and B. Huber, *ChemPhysChem*, 2006, **7**, 2339–2345.

12 S. Bari, P. Sobocinski, J. Postma, F. Alvarado, R. Hoekstra, V. Bernigaud, B. Manil, J. Rangama, B. Huber and T. Schlatholter, *The Journal of Chemical Physics*, 2008, **128**, 074306.

13 S. Bari, R. Hoekstra and T. Schlathölter, *Phys. Chem. Chem. Phys.*, 2010, **12**, 3376–3383.

14 S. Bari, O. Gonzalez-Magaña, G. Reitsma, J. Werner, S. Schippers, R. Hoekstra and T. Schlathölter, *The Journal of Chemical Physics*, 2011, **134**, 024314.

15 F. Calegari, D. Ayuso, A. Trabattoni, L. Belshaw, S. De Camillis, S. Anumula, F. Frassetto, L. Poletto, A. Palacios, P. Decleva, J. B. Greenwood, F. Martín and M. Nisoli, *Science*, 2014, **346**, 336–339.

16 F. Allum, M. Burt, K. Amini, R. Boll, H. Köckert, P. K. Olshin, S. Bari, C. Bomme, F. Braußе, B. Cunha de Miranda, S. Düsterer, B. Erk, M. Géléoc, R. Geneaux, A. S. Gentleman, G. Goldsztejn, R. Guillemin, D. M. P. Holland, I. Ismail, P. Johnsson, L. Journel, J. Küpper, J. Lahl, J. W. L. Lee, S. Maclot, S. R. Mackenzie, B. Manschwetus, A. S. Mereshchenko, R. Mason, J. Palaudoux, M. N. Piancastelli, F. Penent, D. Rompotis, A. Rouzée, T. Ruchon, A. Rudenko, E. Savelyev, M. Simon, N. Schirmel, H. Stapelfeldt, S. Techert, O. Travnikova, S. Trippel, J. G. Underwood, C. Vallance, J. Wiese, F. Ziaee, M. Brouard, T. Marchenko and D. Rolles, *The Journal of Chemical Physics*, 2018, **149**, 204313.

17 S. Bari, D. Egorov, T. L. C. Jansen, R. Boll, R. Hoekstra, S. Techert, V. Zamudio-Bayer, C. Bülow, R. Lindblad, G. Leistner, A. Ławicki, K. Hirsch, P. S. Miedema, B. von Issendorff, J. T. Lau and T. Schlathölter, *Chemistry – A European Journal*, 2018, **24**, 7631–7636.

18 L. Schwob, S. Dörner, K. Atak, K. Schubert, M. Timm, C. Bülow, V. Zamudio-Bayer, B. von Issendorff, J. T. Lau, S. Techert and S. Bari, *The Journal of Physical Chemistry Letters*, 2020, **11**, 1215–1221.

19 S. Maclot, D. G. Piekarski, A. Domaracka, A. Mery, V. Vizcaino, L. Adoui, F. Martín, M. Alcamí, B. A. Huber, P. Rousseau and S. Diaz-Tendero, *J. Phys. Chem. Lett.*, 2013, **4**, 3903–3909.

20 S. Maclot, D. G. Piekarski, R. Delaunay, A. Domaracka, A. Méry, V. Vizcaino, J.-Y. Chesnel, F. Martín, M. Alcamí, B. A. Huber, L. Adoui, P. Rousseau and S. Díaz-Tendero, *The European Physical Journal D*, 2014, **68**, 149.

21 M. Capron, S. Diaz-Tendero, S. MacLot, A. Domaracka, E. Lattouf, A. Lawicki, R. Maisonny, J. Y. Chesnel, A. Mery, J. C. Poully, J. Rangama, L. Adoui, F. Martin, M. Alcami, P. Rousseau and B. A. Huber, *Chemistry - A European Journal*, 2012, **18**, 9321–9332.

22 D. G. Piekarski, R. Delaunay, A. Mika, S. Maclot, L. Adoui, F. Martin, M. Alcami, B. A. Huber, P. Rousseau, S. Diaz-Tendero and A. Domaracka, *Phys. Chem. Chem. Phys.*, 2017, **19**, 19609–19618.

23 D. G. Piekarski, R. Delaunay, S. Maclot, L. Adoui, F. Martín, M. Alcamí, B. A. Huber, P. Rousseau, A. Domaracka and S. Díaz-Tendero, *Phys. Chem. Chem. Phys.*, 2015, **17**, 16767–16778.

24 *Radioprotective Agents*, American Cancer Society, 2006.

25 E. A. Varanda and D. C. Tavares, *Journal of Venomous Animals and Toxins*, 1998, **4**, 5 – 21.

26 S. Abou-Zeid, B. EL-bialy, N. EL-borai, H. AbuBarkr and A. Elhadary, *Sci Rep*, 2018, **8**, 7423.

27 J. Reisz, N. Bansal, J. Qian, W. Zhao and C. Furdui, *Antioxidants & Redox Signaling*, 2014, **21**, 260–292.

28 J. Roberts, *Amino Acids*, 1992, **3**, 25–52.

29 K. H. Dittmann, N. Gueven, C. Mayer and H.-P. Rodemann, *Protein Engineering, Design and Selection*, 2001, **14**, 157–160.

30 R. Marcuse, *Nature*, 1960, **186**, 886–887.

31 R. Marcuse, *Journal of the American Oil Chemists' Society*, 1962, **39**, 97–103.

32 E. Y. Park, H. Murakami and Y. Matsumura, *Journal of Agricultural and Food Chemistry*, 2005, **53**, 8334–8341.

33 W. Wang and E. G. De Mejia, *Comprehensive Reviews in Food Science and Food Safety*, 2005, **4**, 63–78.

34 B. H. Sarmadi and A. Ismail, *Peptides*, 2010, **31**, 1949–1956.

35 M. Memarpoor-Yazdi, H. Mahaki and H. Zare-Zardini, *Journal of Functional Foods*, 2013, **5**, 62–70.

36 M. Pazos, M. L. Andersen and L. H. Skibsted, *Journal of Agricultural and Food Chemistry*, 2006, **54**, 10215–10221.

37 A. Amiri, M. Memarpoor-Yazdi, M. Shanbedi and H. Eshghi, *Journal of Biomedical Materials Research Part A*, 2013, **101A**, 2219–2228.

38 T. T. N. Tran, D. P. Tran, V. C. Nguyen, T. D. T. Tran, T. T. T. Bui and J. H. Bowie, *Journal of Peptide Science*, 2021, **27**, e3295.

39 J. Chatterjee, F. Rechenmacher and H. Kessler, *Angewandte Chemie International Edition*, 2013, **52**, 254–269.

40 M. Mindt, J. Risse, H. Gruss, N. Sewald, E. B.J. and W. V.F., *Sci.Rep.*, 2018, **8**, 12895.

41 I. Lindberg and J. Peinado, in *Encyclopedia of Cell Biology*, ed. R. A. Bradshaw and P. D. Stahl, Academic Press, Waltham, 2016, pp. 84 – 90.

42 A. Sharma, A. Kumar, S. A. H. Abdel Monaim, Y. E. Jad, A. El-Faham, B. G. de la Torre and F. Albericio, *Biopolymers*, 2018, **109**, e23110.

43 Y. Chen, *Chemistry – A European Journal*, 2019, **25**, 3405–3439.

44 S. M. Miller, R. J. Simon, S. Ng, R. N. Zuckermann, J. M. Kerr and W. H. Moos, *Drug Development Research*, 1995, **35**, 20–32.

45 J. M. Ostresh, G. M. Husar, S. E. Blondelle, B. Dörner, P. A. Weber and R. A. Houghten, *Proceedings of the National Academy of Sciences*, 1994, **91**, 11138–11142.

46 P. E. Brown, *Nature*, 1967, **213**, 363–364.

47 R. Reliene, J. M. Pollard, Z. Sobol, B. Trouiller, R. A. Gatti and R. H. Schiestl, *Mutation Research/Fundamental and Molecular Mechanisms of Mutagenesis*, 2009, **665**, 37–43.

48 F. Allaveisi, B. Hashemi and S. M. J. Mortazavi, *Cell and Tissue*

*Banking*, 2015, **16**, 97–108.

49 T. A. Smith, D. R. Kirkpatrick, S. Smith, T. K. Smith, T. Pearson, A. Kailasam, K. Z. Herrmann, J. Schubert and D. K. Agrawal, *Journal of Translational Medicine*, 2017, **15**, 232.

50 T. Shimizu, M. Iwanaga, A. Yasunaga, Y. Urata, S. Goto, S. Shibata and T. Kondo, *Cellular and Molecular Neurobiology*, 1998, **18**, 299–310.

51 K. D. Corbin and S. H. Zeisel, *Current opinion in gastroenterology*, 2012, **28**, 159.

52 D. G. Piekarski and S. Diaz-Tendero, *Phys. Chem. Chem. Phys.*, 2017, **19**, 5465–5476.

53 H. Kasai and K. Kawai, *Chemical research in toxicology*, 2009, **22**, 984–989.

54 V. Bernigaud, O. Kamalou, A. Lawicki, M. Capron, R. Maisonny, B. Manil, L. Maunoury, J. Rangama, P. Rousseau, J. Y. Chesnel, L. Adoui and B. A. Huber, *Publications de l'Observatoire Astronomique de Beograd*, 2008, **84**, 83–86.

55 T. Bergen, X. Biquard, A. Brenac, F. Chandezon, B. A. Huber, D. Jalabert, H. Lebius, M. Maurel, E. Monnand, J. Opitz, A. Pesnelle, B. Pras, C. Ristori and J. C. Rocco, *Rev. Sci. Instrum.*, 1999, **70**, 3244–3253.

56 C. Lee, W. Yang and R. G. Parr, *Phys. Rev. B*, 1988, **37**, 785–789.

57 A. D. Becke, *The Journal of Chemical Physics*, 1993, **98**, 5648–5652.

58 P. J. Stephens, F. J. Devlin, C. F. Chabalowski and M. J. Frisch, *The Journal of Physical Chemistry*, 1994, **98**, 11623–11627.

59 R. Krishnan, J. S. Binkley, R. Seeger and J. A. Pople, *J. Chem. Phys.*, 1980, **72**, 650–654.

60 T. Clark, J. Chandrasekhar, G. W. Spitznagel and P. V. R. Schleyer, *J. Comput. Chem.*, 1983, **4**, 294–301.

61 S. S. Iyengar, H. B. Schlegel, J. M. Millam, G. A. Voth, G. E. Scuseria and M. J. Frisch, *The Journal of Chemical Physics*, 2001, **115**, 10291–10302.

62 H. B. Schlegel, J. M. Millam, S. S. Iyengar, G. A. Voth, A. D. Daniels, G. E. Scuseria and M. J. Frisch, *The Journal of Chemical Physics*, 2001, **114**, 9758–9763.

63 H. B. Schlegel, S. S. Iyengar, X. Li, J. M. Millam, G. A. Voth, G. E. Scuseria and M. J. Frisch, *The Journal of Chemical Physics*, 2002, **117**, 8694–8704.

64 G. Martinet, S. Díaz-Tendero, M. Chabot, K. Wohrer, S. D. Negra, F. Mezdari, H. Hamrita, P. Désesquelles, A. L. Padellec, D. Gardés, L. Lavergne, G. Lalu, X. Grave, J. F. Clavelin, P. A. Hervieux, M. Alcamí and F. Martín, *Phys. Rev. Lett.*, 2004, **93**, 063401.

65 S. Díaz-Tendero, P.-A. Hervieux, M. Alcamí and F. Martín, *Phys. Rev. A*, 2005, **71**, 033202.

66 S. Díaz-Tendero, G. Sanchez, P.-A. Hervieux, M. Alcamí and F. Martín, *Brazilian Journal of Physics*, 2006, **36**, 529 – 533.

67 M. Chabot, G. Martinet, F. Mezdari, S. Diaz-Tendero, K. Béroff-Wohrer, P. Désesquelles, S. Della-Negra, H. Hamrita, A. LePadellec, T. Tuna, L. Montagnon, M. Barat, M. Simon and I. Ismaïl, *Journal of Physics B: Atomic, Molecular and Optical Physics*, 2006, **39**, 2593–2603.

68 L. Chen, S. Martin, J. Bernard and R. Brédy, *Phys. Rev. Lett.*, 2007, **98**, 193401.

69 A. Rentenier, L. F. Ruiz, S. Díaz-Tendero, B. Zarour, P. Moretto-Capelle, D. Bordenave-Montesquieu, A. Bordenave-Montesquieu, P. A. Hervieux, M. Alcamí, M. F. Politis, J. Hanssen and F. Martín, *Phys. Rev. Lett.*, 2008, **100**, 183401.

70 H. da Silva, J. Oller, M. Gatchell, M. H. Stockett, P.-A. Hervieux, L. Adoui, M. Alcamí, B. A. Huber, F. Martín, H. Cederquist, H. Zettergren, P. Rousseau and S. Díaz-Tendero, *Phys. Rev. A*, 2014, **90**, 032701.

71 S. Maclot, R. Delaunay, D. G. Piekarski, A. Domaracka, B. A. Huber, L. Adoui, F. Martín, M. Alcamí, L. Avaldi, P. Bolognesi, S. Díaz-Tendero and P. Rousseau, *Phys. Rev. Lett.*, 2016, **117**, 073201.

72 E. Erdmann, N. F. Aguirre, s. Indrajith, J. Chiarinelli, A. Domaracka, P. Rousseau, B. A. Huber, P. Bolognesi, R. Richter, L. Avaldi, S. Díaz-Tendero, M. Alcami and M. Łabuda, *Phys. Chem. Chem. Phys.*, 2020, –.

73 M. J. Frisch, G. W. Trucks, H. B. Schlegel, G. E. Scuseria, M. A. Robb, J. R. Cheeseman, G. Scalmani, V. Barone, B. Mennucci, G. A. Petersson, H. Nakatsuji, M. Caricato, X. Li, H. P. Hratchian, A. F. Izmaylov, J. Bloino, G. Zheng, J. L. Sonnenberg, M. Hada, M. Ehara, K. Toyota, R. Fukuda, J. Hasegawa, M. Ishida, T. Nakajima, Y. Honda, O. Kitao, H. Nakai, T. Vreven, J. A. Montgomery, Jr., J. E. Peralta, F. Ogliaro, M. Bearpark, J. J. Heyd, E. Brothers, K. N. Kudin, V. N. Staroverov, R. Kobayashi, J. Normand, K. Raghavachari, A. Rendell, J. C. Burant, S. S. Iyengar, J. Tomasi, M. Cossi, N. Rega, J. M. Millam, M. Klene, J. E. Knox, J. B. Cross, V. Bakken, C. Adamo, J. Jaramillo, R. Gomperts, R. E. Stratmann, O. Yazyev, A. J. Austin, R. Cammi, C. Pomelli, J. W. Ochterski, R. L. Martin, K. Morokuma, V. G. Zakrzewski, G. A. Voth, P. Salvador, J. J. Dannenberg, S. Dapprich, A. D. Daniels, Ö. Farkas, J. B. Foresman, J. V. Ortiz, J. Cioslowski and D. J. Fox, *Gaussian 09 Revision B.01*, 2010, Gaussian Inc. Wallingford CT 2009.

74 A. D. Headley and S. D. Starnes, *Journal of Molecular Structure: THEOCHEM*, 1996, **370**, 147 – 155.

75 A. Gómez-Zavaglia and R. Fausto, *Vibrational Spectroscopy*, 2003, **33**, 105 – 126.

76 S. Tian, *The Journal of chemical physics*, 2006, **123**, 244310.

77 H. Guo, L. Zhang, L. Deng, L. Jia, Y. Pan and F. Qi, *The Journal of Physical Chemistry A*, 2010, **114**, 3411–3417.

78 J. G. Herman and S. B. Baylin, *New England Journal of Medicine*, 2003, **349**, 2042–2054.

79 M. Esteller, P. G. Corn, S. B. Baylin and J. G. Herman, *Cancer Research*, 2001, **61**, 3225–3229.

80 K. E. Kruglyakova, B. P. Ulanov, D. L. Zybina and N. M. Emanuel, *Dokl. Akad. Nauk SSSR*, 1965, **161**, 718–720.

81 V. Selezneva, A. Chmarin, T. Golitsyna and D. Zhuk, *Bulletin of the Academy of Sciences of the USSR, Division of chemical science*, 1975, **24**, 189–189.

82 N. Kling, S. Díaz-Tendero, R. Obaid, M. R. Disla, M. Xiong, H. Sundberg, S. Khosravi, M. Davino, P. Drach, A. Carroll, T. Osipov, F. Martin and B. N., *Nat. Commun.*, 2019, **10**, 2813.

83 M. McDonnell, A. C. LaForge, J. Reino-Gonzalez, M. Disla, N. G. Kling, D. Mishra, R. Obaid, M. Sundberg, V. Svoboda, S. Díaz-Tendero, F. Martín and N. Berrah, *J. Phys. Chem. Lett.*, 2020, **11**, 6724–6729.

84 J. Kocisek, D. Piekarski, R. Delaunay, B. Huber, L. Adoui, F. Martin, M. Alcami, P. Rousseau, A. Domaracka, J. Kopyra and S. Díaz-Tendero, *The journal of physical chemistry. A*, 2015, **119**,.

85 O. González-Magaña, M. Tiemens, G. Reitsma, L. Boschman, M. Door, S. Bari, P. O. Lahaie, J. R. Wagner, M. A. Huels, R. Hoekstra and T. Schlathölter, *Phys. Rev. A*, 2013, **87**, 032702.

86 M. Dizdaroglu, *Free Radical Biology and Medicine*, 1991, **10**, 225–242.

87 P. Riley, *International Journal of Radiation Biology*, 1994, **65**, 27–33.

88 J. Cadet, T. Douki and J.-L. Ravanat, *Free Radic Biol Med*, 2010, **49**, 9–21.

89 S. S. Wallace, *Radiation Research*, 1998, **150**, S60—-S79.